A Truncated Fourier Based Analytical Model for SRMs with Higher Number of Rotor Poles

Zichao Jin, Yijiang Jia, Mohamad Salameh, Berker Bilgin, Shuwang Li, Mahesh Krishnamurthy
Electric Drives and Energy Conversion Laboratory
Illinois Institute of Technology, Chicago, IL 60616 USA
EML: kmahesh@iit.edu; URL: http://drives.ece.iit.edu

***Abstract*- Switched reluctance motors (SRM) have been seen as a potential candidate for automotive, aerospace as well as domestic applications and High-Rotor pole SRM (HR-SRM) present a significant advancement in this area. This machine configuration offers most of the the benefits offered by conventional SRMs and has shown significant benefits in efficiency and torque quality. However, HR-SRM has a narrower inductance profile with a lower saliency ratio as compared to a conventional SRM with an identical stator. This can make it inherently challenging to directly adopt mathematical models and sensorless control approaches currently in use. This paper presents a time-efficient analytical model for the characterization of a 6/10 SRM using an inductance model utilizing truncated Fourier series as well as multi-order polynomial curve-fitting algorithm. The inductance model is extended to accurately predict back-EMF and electromagnetic torque response towards obtaining a comprehensive model for every operating point of the machine during dynamic operation. The effectiveness of the proposed concept has analyzed for a prototype machine and verified using Finite Element Analysis (FEA).**

***Keywords*— Switched relucatance machine, analytical model, finite element methods, electric motors.**

I. INTRODUCTION

A Switched Reluctance Machine (SRM) has simple construction with low manufacturing cost and maintenance. Moreover, it has a very wide speed range and is capable of operating in harsh environments, such as high temperatures and severe vibration because of the absence of permanent magnets or windings in the rotor [1]-[5]. In spite of these benefits, conventional SRMs have faced challenges in terms of high acoustic noise and torque ripple [6]-[12]. Further, the double saliency structure renders its inductance, back-EMF and torque profiles highly nonlinear, which significantly increases the complexity of modeling and driving the machine [13]-[14]. With the primary purpose of reducing the torque ripple, improving average torque and efficiency of the SRM, an SRM with higher number of rotor poles than the number of stator poles has been introduced in [15]. The 6/10 configuration has been compared the 6/4 machine in [15] and 6/8 SRM [16]. Compared to the conventional configurations, the high rotor pole model has been shown to have an improvement of 28.6% in continuous current ratings, 25% and 20% in peak and average torque.

In order to implement a high-efficiency SRM drive system for high-performance applications such as vehicle propulsion systems or servo drives, an accurate and efficient analytical model of the machine is required for real-time control, fault diagnostics, survivable operation and sensorlss control. The main purpose of modeling inductance/flux linkage to characterize performance of the SR machine is to reduce the data reliance whenever a machine representation is needed. Methods to model inductance of an SRM have been well-established using two main approaches introduced in [17] and [18]. Authors in [17] presented a generalized model that covers most SRMs. Material properties and geometry-based equations are utilized in this modeling technique in order to replace the FEA simulation or hardware measurement and this methodology requires the mechanical and geometrical information from the machine manufacturer. In [18], a high-performance modeling technique has been proposed for conventional 8/6 SR machine, which uses a data acquisition process to initialize the model either by FEA simulation or hardware measurement.

Since inductance is dependant on the phase current and rotor position, different analytical tools are required in modeling these two independent variables. In general, the most effective way of modeling the inductance of SRM with respect to rotor position is utilizing truncated Fourier series, which is used in both the SRM model for specific stator/rotor configuration [18] and the generalized machine model for all types of SRMs [17]. The inductance of SRM with respect to different phase current values and rotor positions can be expressed as the following [18]:

$$L(\theta, i) = \sum_{n=0}^{\infty} L_n(i) \cos(n(N_r \theta + \varphi_k)) \quad (1)$$

Where n and N_r corresponds to the number of components of the Fourier series and number of rotor poles.

The introduction of $L_n(i)$ is done mainly to obtain the relationship between the inductance and phase current. In [18], this function is solved using multiple order polynomial curve-fitting routines. By sampling dozens of points of inductance for different values of current at a specific critical positions of the 8/6 SRM, inductance curves as a functions of the phase current and position can be obtained. These curves are used to identify $L_n(i)$.

This paper presents a mathematical model for an SRM using a truncated Foureier series approach. Four key rotor positions are identified that are used to formulate coefficients of the mathematical model of the SRM. Once calibrated, this model can be used to develop a dynamic behavioral model at any rotor position and for any value of current.

II. MODELING FUNDAMENTALS FOR A 6/10 HR-SRM

A. Model Identification

The most effective approach for modeling the inductance of an SRM with respect to rotor position is by utilizing truncated Fourier series. However, the number of terms of this Fourier series is be determined by the number of desired sampling positions. In a conventional 8/6 SRM, such positions are selected based on the geometric feature of itself; while in the high rotor pole 6/10 design, one cannot obtain the same number of sampling positions. As shown in Fig. 1, when Phase A of the 6/10 SR machine is in fully aligned position, the electrical angle of Phase B and Phase C are 60° and 300°. On the other hand, when Phase A is in fully unaligned position, the electrical angle of Phase B and Phase C are 120° and 240°, respectively. This configuration leads to four sampling positions, starting with alignment of a phase with a rotor pole pair as well as aligning this phase with the bisector of two rotor pole pairs.

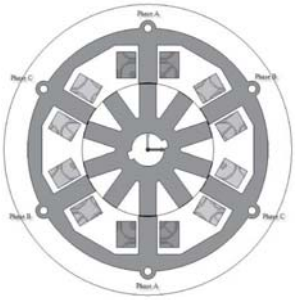

Fig. 1(a). Sampling position for 6/10 SRM aligned position.

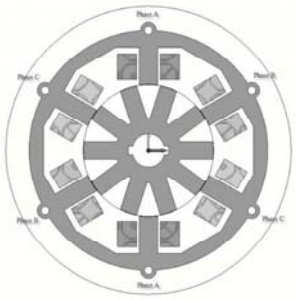

Fig. 1(b). Sampling position for 6/10 SRM aligned position.

Four specific positions of the 6/10 SR machine are considered during the data acquisition process, which includes the fully aligned position, 60º electrical angle position, 120º electrical angle position and fully unaligned position. One could acquire two positions for the measurement by aligning one of the phases to a rotor pole pair or to a bisector between two rotor pole pairs; therefore, the locked shaft needs to be adjusted from the fully aligned/unaligned position for one phase to the opposite position of this phase during the whole measurement procedure. In addition, the number of points as well as the step size of the inductance with respect to different phase current values can be determined based on the current range of the machine.

Due to the geometric construction of the 6/10 SRM, one cannot obtain the fully unaligned position of the machine without any precise position control technique at standstill; therefore, a rotary indexer is needed to obtain the fully unaligned position as well as to prevent the shaft/rotor from moving during the measurement. The indexer should be capable of handling the maximum operating electromagnetic torque of the machine.

With these four sampling positions, the number of terms of the Fourier series has been set to four. The expression of the inductance of 6/10 SRM can be expressed as:

$$\begin{aligned} L(\theta,i) &= L_0(i) + L_1(i)\cos(10\theta+\varphi_k) \\ &\quad + L_2(i)\cos(20\theta+2\varphi_k) \\ &\quad + L_3(i)\cos(30\theta+3\varphi_k) \end{aligned} \tag{2}$$

where θ, i, φ_k denote the rotor position, phase current and phase shift respectively. Functions $L_0(i)$ to $L_3(i)$ can be expressed by the inductance at the four sampling positions as shown in the (3), where $L_a(i)$, $L_b(i)$, $L_c(i)$ and $L_d(i)$ refer to the inductance in the fully aligned position, 120° electrical angle position, 60° electrical angle position and fully unaligned position, respectively. The inductance curves can be obtained by curve fitting routines of the multiple order polynomial function, $L_a(i)=\sum_{n=0}^{k} a_n i^n$, $L_b(i)$, $L_c(i)$ and $L_c(i)$ are expressed in same way as $\sum_{n=0}^{k} b_n i^n$, $\sum_{n=0}^{k} c_n i^n$, $\sum_{n=0}^{k} d_n i^n$, as shown in Fig. 2. It should be noted that both $L_0(i)$ to $L_3(i)$ and $L_a(i)$ to $L_u(i)$ are functions of the phase current; however, only $L_a(i)$ to $L_u(i)$ have physical significance. Accordingly, the inductance expressions can be used to determine the back-emf of the machine as shown in (4). Similarly, the developed torque can be computed using the co-energy principle.

$$\frac{1}{6}\begin{pmatrix} 1 & 2 & 2 & 1 \\ 2 & 2 & -2 & -2 \\ 2 & -2 & -2 & 2 \\ 1 & -2 & 2 & -1 \end{pmatrix}\begin{pmatrix} L_a(i) \\ L_b(i) \\ L_c(i) \\ L_u(i) \end{pmatrix}=\begin{pmatrix} L_0(i) \\ L_1(i) \\ L_2(i) \\ L_3(i) \end{pmatrix} \tag{3}$$

$$\begin{aligned} E_b &= \omega i \frac{dL(\theta,i)}{d\theta} \\ &= \omega i \frac{d[L_0(i)+L_1(i)\cos(N_r\theta)+L_2(i)\cos(2N_r\theta)+L_3(i)\cos(3N_r\theta)]}{d\theta} \\ &= \omega i\{-N_r[\frac{1}{3}L_a(i)\sin(N_r\theta)+\frac{1}{3}L_b(i)\sin(N_r\theta)-\frac{1}{3}L_c(i)\sin(N_r\theta)-\frac{1}{3}L_u(i)\sin(N_r\theta)] \\ &\quad -2N_r[\frac{1}{3}L_a(i)\sin(2N_r\theta)-\frac{1}{3}L_b(i)\sin(2N_r\theta)-\frac{1}{3}L_c(i)\sin(2N_r\theta)+\frac{1}{3}L_u(i)\sin(2N_r\theta)] \\ &\quad -3N_r[\frac{1}{6}L_a(i)\sin(3N_r\theta)-\frac{1}{3}L_b(i)\sin(3N_r\theta)+\frac{1}{3}L_c(i)\sin(3N_r\theta)-\frac{1}{6}L_u(i)\sin(3N_r\theta)]\} \end{aligned} \tag{4}$$

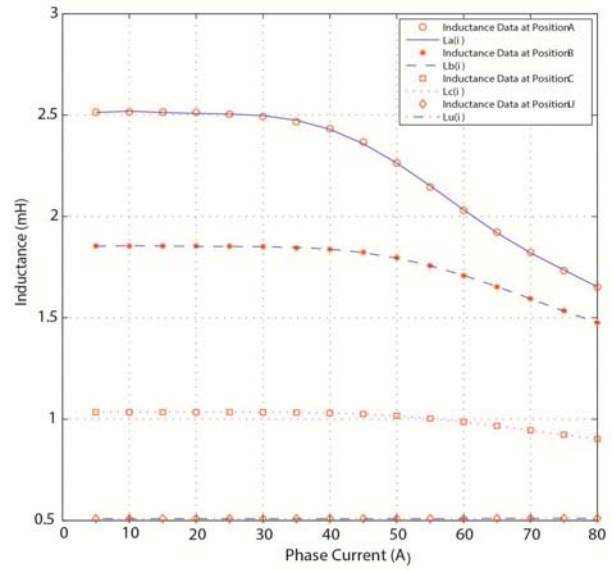

Fig. 2. Inductance as a function of current for different rotor positions.

Inductance of an SRM has a three-dimensional relationship with phase current and rotor position, as shown in Fig. 3. Therefore, the co-energy of SRM can also be considered as a function of these two variables, which can be denoted as, $W'_f(q,i)$, and can be expressed as:

$$W'_f(\theta,i)=\int_0^i L(\theta,i)i di \tag{5}$$

The airgap electromagnetic torque can be calculated using:

$$T_e=\frac{\partial W'_f(\theta,i)}{\partial\theta} \tag{6}$$

By substituting the inductance equation into the electromagnetic torque equation, one could calculate the electromagnetic torque for one phase as in (11), the $L^{\bullet}_a(i)$, $L^{\bullet}_b(i)$, $L^{\bullet}_c(i)$ and $L^{\bullet}_d(i)$ represent the integral function of inductance (a) common divisor i has be extracted), which could be written as:

$$L^{\bullet}_a(i)=\sum_{n=0}^{k}\frac{1}{n+2}a_n i^n \tag{7}$$

$$L^{\bullet}_b(i)=\sum_{n=0}^{k}\frac{1}{n+2}b_n i^n \tag{8}$$

$$L^{\bullet}_c(i)=\sum_{n=0}^{k}\frac{1}{n+2}c_n i^n \tag{9}$$

$$L^{\bullet}_u(i)=\sum_{n=0}^{k}\frac{1}{n+2}u_n i^n \tag{10}$$

B. Inductance Measurement of 5hp HR-SRM Prototype

The most common hardware measurement technique for SR machine is the direct DC test method [19]. In the mentioned method, a voltage pulse is applied on one of the phases of the SRM with its locked rotor is in an identified position until the phase current hits the threshold value. Afterwards, the inductance can be calculated directly from the inspected phase current as well as the magnitude and period of the voltage pulse. Fig. 4 shows the equivalent circuit of the inductance measurement with hardware, where L, R, V_s and i_1 denote inductance, resistance of the phase winding, the source voltage and the phase current, respectively. Fig. 5 shows the hardware setup. The phase current can the phase inductance can be expressed as in (12) and (13).

$$\begin{aligned}
T_e&=\frac{\partial W'_f(\theta,i)}{\partial\theta}\\
&=\frac{\partial\int_0^i L(\theta,i)i di}{\partial\theta}\\
&=\frac{\partial\int_0^i [L_0(i)+L_1(i)\cos(N_r\theta)+L_2(i)\cos(2N_r\theta)+L_3(i)\cos(3N_r\theta)]i di}{\partial\theta}\\
&=-N_r i^2[\frac{1}{3}L^{\bullet}_a(i)\sin(N_r\theta)+\frac{1}{3}L^{\bullet}_b(i)\sin(N_r\theta)-\frac{1}{3}L^{\bullet}_c(i)\sin(N_r\theta)-\frac{1}{3}L^{\bullet}_u(i)\sin(N_r\theta)]\\
&\quad-2N_r i^2[\frac{1}{3}L^{\bullet}_a(i)\sin(2N_r\theta)-\frac{1}{3}L^{\bullet}_b(i)\sin(2N_r\theta)-\frac{1}{3}L^{\bullet}_c(i)\sin(2N_r\theta)+\frac{1}{3}L^{\bullet}_u(i)\sin(2N_r\theta)]\\
&\quad-3N_r i^2[\frac{1}{6}L^{\bullet}_a(i)\sin(3N_r\theta)-\frac{1}{3}L^{\bullet}_b(i)\sin(3N_r\theta)+\frac{1}{3}L^{\bullet}_c(i)\sin(3N_r\theta)-\frac{1}{6}L^{\bullet}_u(i)\sin(3N_r\theta)]
\end{aligned} \tag{11}$$

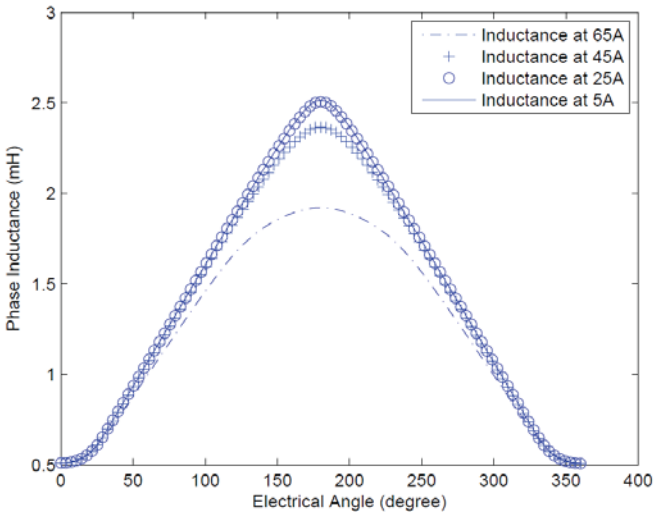

Fig. 3. Inductance profile at different phase currents

$$i_1(t) = \frac{V_s}{R}(1 - e^{-\frac{R}{L}t}) \tag{12}$$

$$L = \frac{Rt}{ln(\frac{V_s}{V_s - Ri_1(t)})} \tag{13}$$

The inductance value with respect to the expected value of the phase current can be obtained by measuring the magnitude as well as the period of the voltage pulse. Only a single leading-edge measurement is needed for a specific rotor position, as shown in Fig. 6, which shows current waveform at 30A and a 60A current.

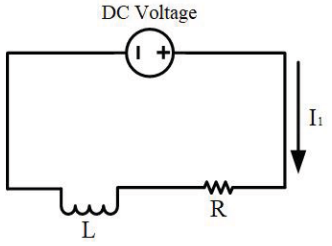

Fig. 4. Equivalent circuit of hardware measurement of inductance at standstill.

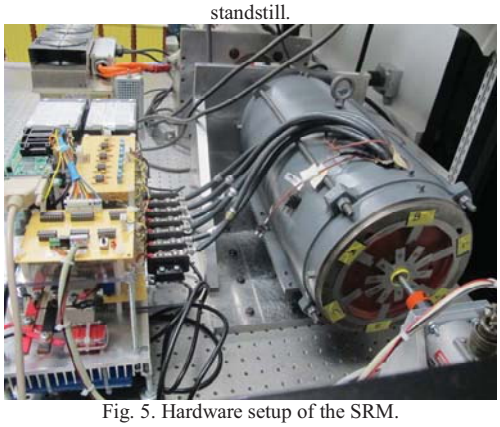
Fig. 5. Hardware setup of the SRM.

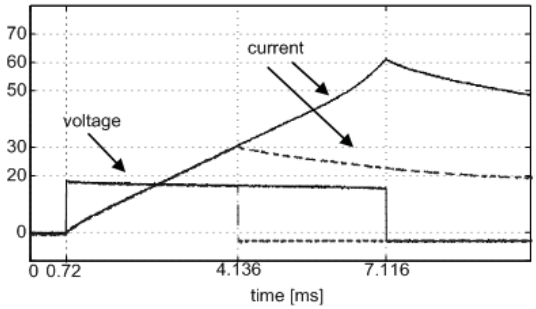

Fig. 6. Inductance measurement for 30A and 60A of phase current

III. INDUCTANCE MODEL VALIDATION

The proposed analytical model of the 6/10 SRM can be incorporated into the dynamic simulation model of the machine drive system, since it does not require additional simulation software environment. This allows a time-efficient model with a considerately high precision that can be extended to any other SRM with the same stator/rotor configuration. A 5 hp 6/10 SRM prototype was used as the target machine for validating the developed model. A co-simulation model was devleoped, where the power electronic components and PI controller blocks in MATLAB/SIMULINK were used to control an FEA model of the target 6/10 SR machine built in MagNet® by Mentor. Another method based on inductance and torque look-up table to analyze the dynamic performance was also carried out. The strengths and weaknesses of the three methods for dynamic simualtion of the 6/10 SRM is shown in table 1. As shown in Fig. 5 (a)-(c), the model validation results show a good match with the actual results. Furthermore, the results from the dynamic co-simulation of the drive system agrees with the results obtained using the developed model, as shown in Fig. 5 (d)-(e).

TABLE I
COMPRISON OF THE DIFFERENT SOLUTIONS FOR DYNAMIC SIMULATION

Evaluation Criteria	Co-Simualtion Model	Look-up Table Based Model	Proposed Analytical Model
Resource Consumption	High	Low	Low
System Complexity	High	Low	High
Extension Difficulty	High	High	Low
Elapsed Simulation Time	High	Low	Moderate
Storage Space Requirement	High	Moderate	Low
Simulation Results Error Level	Low	High	Low

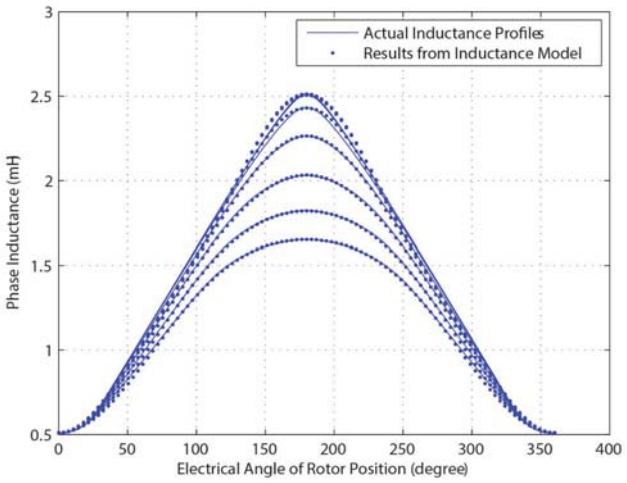

(a)

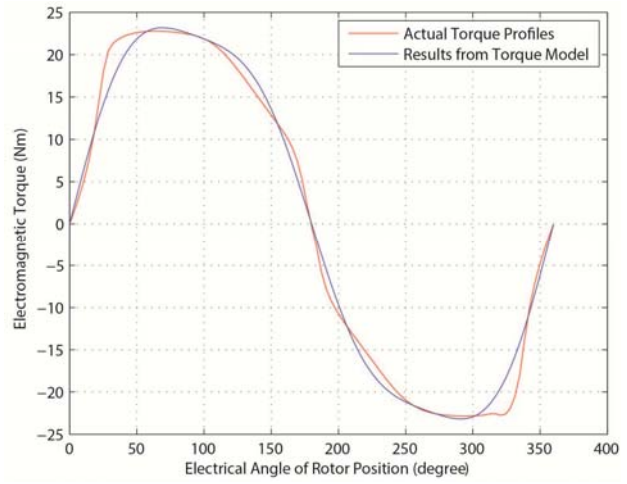

(b)

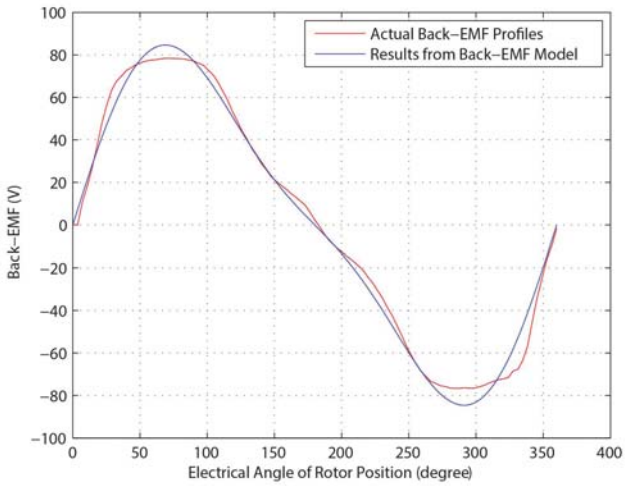

(c)

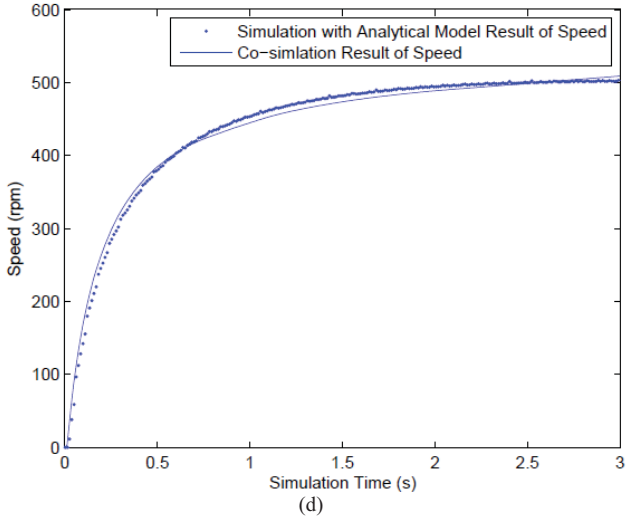

(d)

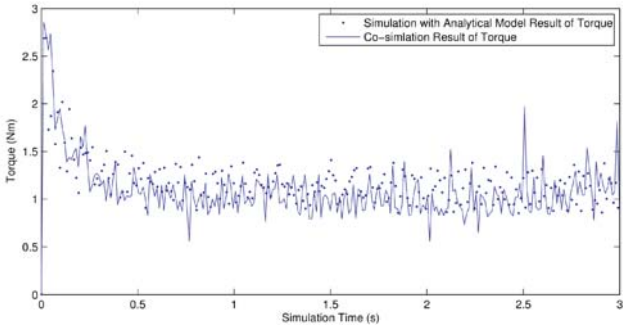

(e)

Fig. 5. Model validation results (a) Inductance profile (b) Torque profile at 80 A (c) Back-emf profile at 80 A (d) speed - dynamic response (e) torque - dynamic response.

In order to quantify the error of inductance model, a Mean Absolute Percentage Error (MAPE) was calculated, the MAPE is expressed as:

$$MAPE = \frac{100\%}{n}\sum_{t=1}^{n}\left|\frac{A_t - F_t}{A_t}\right| \tag{14}$$

where A_t and F_t are the actual value and forecast value respectively. Fig. 6 (a) indicates the the variation of error along different phase current level. One could infer that the error of the model reduces significantly at higher current level. This phenomenon can be attributed to the truncated Fourier series used in modeling the relationship between phase inductance and rotor position. Since the phase inductance profile of the SRM is increasingly close to a sinusoidal waveform when the phase current gets into the saturation region of the machine, and the truncated Fourier series is mathematically expressed as a sinusoid-based series, the modeling error with respect to rotor position would decrease with the increasing phase current. Fig. 6 (b) shows the relationship between error of the model and rotor position. In this figure, one can easily recognize the sampling positions of the inductance data acquisition, which is the position at 0◦ (equivalent to 360º as fully aligned position), 30º (equivalent

to 330º) , 120º (equivalent to 240º and 180º of electrical angle (fully aligned position), since the error around these positions are relatively lower.

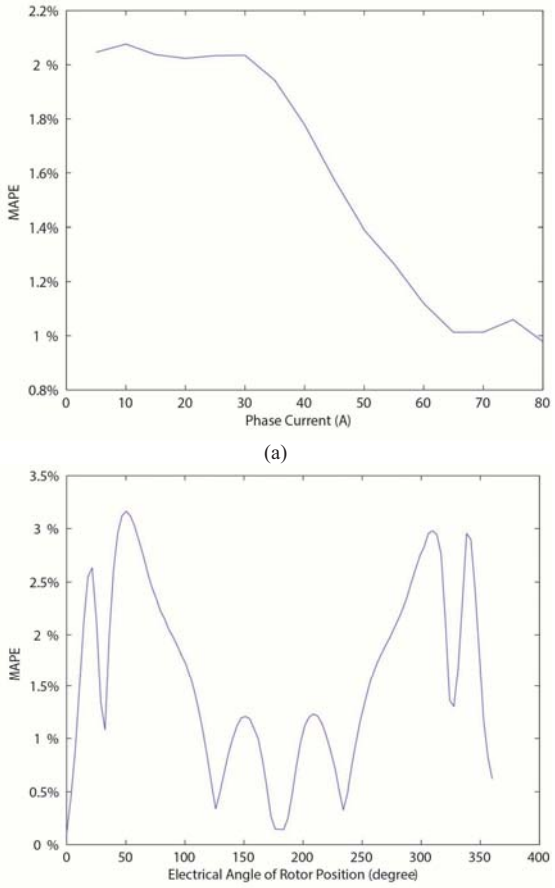

Fig. 6. Error variation of the inductance model for (a) different phase current level and (b) different rotor position.

IV. CONCLUSIONS AND FUTURE WORK

This work proposes an analytical model for a high-rotor pole 6/10 SRM. The machine model is derived from an analytical inductance model utilizing truncated Fourier series as well as multi-order polynomial curve-fitting routines. This approach can be used to develop a detailed behavioral model towards the design and implementation of the SRM drive for any operating point. This model was found to be effective in predicting dynamic behavior of the machine using a small set of inductance measurements obtained and stored offline. This machine configuration does not allow the direct measurement of inductance coefficients at specific points of interest from a single position, which is possible for a conventional 8/6 SRM. This limitation necessitates the use of a rotary indexer to lock the shaft/rotor during the inductance measurement to obtain fully unaligned position of the 6/10 SRM for accurate inductance calibration from a hardware setup.

The validation results of the model show a good match with the actual simulation results, the maximum MAPE was nearly 3.1%.

ACKNOWLEDGMENT

This work was supported in part by the U.S. National Science Foundation under Grant 1927432.

REFERENCES

[1] M. Krishnamurthy, C. S. Edrington, A. Emadi, P. Asadi, M. Ehsani, and B. Fahimi, "Making the case for applications of switched reluctance motor technology in automotive products," IEEE Trans. Power Electron., vol. 21, no. 3, pp. 659–675, May 2006.

[2] B. Fahimi, A. Emadi, and R. B. Sepe, Jr., "Four-quadrant position sensorless control in SRM drives over entire speed range," IEEE Trans. Power Electron., vol. 20, no. 1, pp. 154–163, Jan. 2005.

[3] P. N.Materu and R. Krishnan, "Steady-state analysis of the variable-speed switched reluctance motor drive," IEEE Trans. Ind. Electron., vol. 36, no. 4, pp. 523–529, Nov. 1989.

[4] C. Mademlis and I. Kioskeridis, "Gain-scheduling regulator for high performance position control of switch reluctance motor drives," IEEE Trans. Ind. Electron., vol. 57, no. 9, pp. 2922–2931, Sep. 2010.

[5] K. Ha, C. Lee, J. Kim, R. Krishnan, and S.-G. Oh, "Design and development of low-cost and high-efficiency variable-speed drive system with switched reluctance motor," IEEE Trans. Ind. Appl., vol. 43, no. 3, pp. 703–713, May/Jun. 2007.

[6] A. M. Stankovic, G. Tadmor, Z. J. Coric, and I. Agirman, "On torque ripple reduction in current-fed switched reluctance motors," IEEE Trans. Ind. Electron., vol. 46, no. 1, pp. 177–183, Feb. 1999.

[7] M. S. Islam and I. Husain, "Torque-ripple minimization with indirect position and speed sensing for switched reluctance motors," IEEE Trans. Ind. Electron., vol. 47, no. 5, pp. 1126–1133, Oct. 2000.

[8] J.-W. Ahn, S.-J. Park, and D.-H. Lee, "Hybrid excitation of SRM for reduction of vibration and acoustic noise," IEEE Trans. Ind. Electron., vol. 51, no. 2, pp. 374–380, Apr. 2004.

[9] I. Husain, "Minimization of torque ripple in SRM drives," IEEE Trans. Ind. Electron., vol. 49, no. 1, pp. 28–39, Feb. 2002.

[10] F. C. Lin and S.-M. Yang, "An approach to producing controlled radial force in a switched reluctance motor," IEEE Trans. Ind. Electron., vol. 54, no. 4, pp. 2137–2146, Aug. 2007.

[11] J. O. Fielder, K. A. Kasper, and R. W. De Doncker, "Calculation of the acoustic noise spectrum of SRM using modal superposition," IEEE Trans. Ind. Electron., vol. 57, no. 9, pp. 2939–2945, Sep. 2010.

[12] M. van der Giet, E. Lange, D. A. P. Correa, I. E. Chabu, S. I. Nabeta, and K. Hameyer, "Acoustic simulation of a special switched reluctance drive by means of field-circuit coupling and multiphysics simulation," IEEE Trans. Ind. Electron., vol. 57, no. 9, pp. 2946–2953, Sep. 2010.

[13] R. Krishnan, Switched Reluctance Motor Drives Modeling, Simulation, Analysis, Design and Applications. Boca Raton, FL: CRC, 2001.

[14] I. Husain and S. A. Hossain, "Modeling, simulation, and control of switched reluctance motor drives," IEEE Trans. Ind. Electron., vol. 52, no. 6, pp. 1625–1634, Dec. 2005.

[15] P. C. Desai, M. Krishnamurthy, N. Schofield and A. Emadi, "Design and performance evaluation of a novel 6/10 Switched Reluctance Machine," 2009 IEEE International Electric Machines and Drives Conference, Miami, FL, 2009, pp. 755-762.

[16] B. Bilgin, A. Emadi and M. Krishnamurthy, "Design Considerations for Switched Reluctance Machines With a Higher Number of Rotor Poles," in IEEE Transactions on Industrial Electronics, vol. 59, no. 10, pp. 3745-3756, Oct. 2012.

[17] A. Khalil and I. Husain, "A Fourier series generalized geometry based analytical model of switched reluctance machines," IEEE International Conference on Electric Machines and Drives, 2005., San Antonio, TX, 2005, pp. 490-497.

[18] B. Fahimi, G. Suresh, J. Mahdavi and M. Ehsami, "A new approach to model switched reluctance motor drive application to dynamic performance prediction, control and design," PESC 98 Record. 29th Annual IEEE Power Electronics Specialists Conference (Cat. No.98CH36196), Fukuoka, 1998, pp. 2097-2102 vol.2.

[19] R. Krishnan and P. Materu, "Measurement and instrumentation of a switched reluctance motor," Conference Record of the IEEE Industry Applications Society Annual Meeting, San Diego, CA, USA, 1989, pp. 116-121 vol.1.